atmosphere

MDPI

Article

A Comparative Analysis of Changes in Temperature and Precipitation Extremes since 1960 between China and Greece

Zhen Li [1], Yingling Shi [2], Athanassios A. Argiriou [3,*], Panagiotis Ioannidis [3], Anna Mamara [3,4] and Zhongwei Yan [1,5,*]

[1] Key Laboratory of Regional Climate-Environment in Temperate East Asia, Institute of Atmospheric Physics, Chinese Academy of Sciences, Beijing 100029, China
[2] Longyang District Meteorological Service, Baoshan 678007, China
[3] Laboratory of Atmospheric Physics, Department of Physics, University of Patras, 26504 Rio, Greece
[4] Hellenic National Meteorological Service, 16777 Athens, Greece
[5] College of Earth and Planetary Sciences, University of Chinese Academy of Sciences, Beijing 100049, China
* Correspondence: athanarg@upatras.gr (A.A.A.); yzw@tea.ac.cn (Z.Y.)

Abstract: The temporal and spatial variations of 26 extreme temperature and precipitation indices for China and Greece were comparatively analysed. Also, their association with atmospheric circulation types was evaluated using multiple linear regression. The calculation of the extreme indices was based on homogenized daily temperature and precipitation time series from 1960 to 2010 for Greece and 2021 for China. Extreme precipitation, intensity, and short-term heavy precipitation increased, while persistent heavy precipitation has decreased since 1960 in China. Short-term heavy precipitation has also shown an increasing trend in Greece, though total precipitation and persistent heavy precipitation decreased there between 1960 and 2010. Extreme cold events have tended to decrease, and extreme warm events have increased in both countries, a fact that can be attributed to global warming. For comparison, climatic warming in China was mainly seen in the half year of winter, while the extreme indices relevant to cold seasons such as FD0 and ID0 presented a small trend in Greece. The observed changes in many climatic indices, including RX5day and WSDI in China and R20MM, RX5day, CDD, PRCPTOT and FD0 in Greece, could be partly explained by those of the main large-scale circulation types in the corresponding regions. The significant multiple correlation coefficients of the main circulation types were up to 0.53 for RX5day and 0.54 for WSDI in China, and 0.74 for PRCPTOT and 0.71 for R20MM in Greece. The relationships between climatic indices and circulation types were closer in Greece than in China, especially for the precipitation indices.

Keywords: extreme temperature; extreme precipitation; comparative analysis; circulation type; China; Greece

Citation: Li, Z.; Shi, Y.; Argiriou, A.A.; Ioannidis, P.; Mamara, A.; Yan, Z. A Comparative Analysis of Changes in Temperature and Precipitation Extremes since 1960 between China and Greece. *Atmosphere* **2022**, *13*, 1824. https://doi.org/10.3390/atmos13111824

Academic Editor: Thierry Bergot

Received: 4 October 2022
Accepted: 27 October 2022
Published: 2 November 2022

1. Introduction

According to the Intergovernmental Panel for Climate Change (IPCC) sixth assessment report (AR6), each of the last four decades has been progressively warmer in global mean than the preceding decade and the average global surface temperature in the first two decades of the 21st century was 0.99 °C higher than the 1850–1900 mean, while more recently, from 2011 to 2020, it was 1.09 °C warmer than the historic base period [1]. The rising temperature has been accompanied by unprecedented changes of climate extremes, i.e., the frequency and intensity of some extreme weather and climate events have increased and will continue to increase under medium and high emission scenarios. Understanding the changing frequency and severity of extreme events in association with floods, droughts and heatwaves is imperative since the extreme events directly affect human societies and the Earth's ecosystems in different regions.

China and Greece have served as two key nodes in the intercontinental trade zone between Asia and Europe, widely known as the ancient Silk Road. Greece and the Mediterranean domain in general are listed among the climate change hotspots. The same stands also for China, where climate warming has seen nearly a doubling of the global mean rate since 1900 [2], with even more significant local changes such as those over the Tibetan Plateau [3]. In both countries, climate change would pose challenges to vital socioeconomic sectors, such as human health, ecosystems, forestry, agriculture and tourism and international activities between the regions. More than ever, monitoring present-day climate variability is necessary for understanding the impact of climate change on regional and global scales. Within this perspective, it is beneficial to comparatively investigate different regional climate changes, especially dealing with climate extremes between the two countries under global warming. As two basic climatic elements, temperature and precipitation are of primary importance in weather and climate studies. There have been many analyses of the changing temperature and precipitation extremes in China and Greece. Ren et al. [4] found that the extreme indices related to low temperature generally decreased in frequency and intensity while those related to high temperature mostly increased in frequency and intensity. Shi et al. [5] analysed the spatiotemporal trends in temperature extremes and their associations with eight metrics of large-scale circulation patterns in China and the results indicated that the increase in tropical nights (TR20), summer days (SU25), warm days (TX90p) and warm nights (TN90p), concurrently with the decrease in frost days (FD0), ice days (ID0), cool days (TX10p) and cool nights (TN10p) was highly pronounced in China as a whole. Yin et al. [6] calculated 26 extreme temperature and precipitation indices as defined by the Expert Team on Climate Change Detection and Indices (ETCCDI) and analysed the characteristics of extreme temperature and precipitation in China in 2017. Wang and Yan [7] revealed an approximate doubling in both the frequency and the magnitude of regional heat wave events in China between 1960 and 2018. During the modern observation period, most of the extreme precipitation indices (except for the consecutive dry days, CDD) showed increasing trends in Northwest China, the mid–lower reaches of the Yangtze River, the south-eastern coast and South China, but decreasing trends in North China, Northeast China, and parts of Southwest China [8,9]. Pei et al. [10] analysed the contribution of human-induced atmospheric circulation changes to the record-breaking winter precipitation in Beijing. For Greece, some previous studies revealed the changes of extreme temperature events [11,12] and extreme precipitation events [13] and their relationship with large-scale circulation indices or circulation types. Bartzokas and Houssos [11] focused on the extreme temperature events in northwestern Greece in winter and summer between 1970 and 2002 and sought the atmospheric pressure patterns associated with or favouring such events. Houssos and Bartzokas [13] focused on extreme precipitation events covering the same period. Kolios et al. [12] studied the extreme high/low values (EHT/ELT) of temperature in Greece using a 40-year time series and found the positive trends of EHT and ELT frequency of occurrence in most of the stations examined, indicating an environment exposed more and more to extreme air temperature values. Overall, recent studies have drawn attention to the characteristics of extreme climate change in both countries. However, it remains interesting to comparatively investigate the extreme regional climate changes based on updated homogenised daily observations and possible underlying mechanisms.

Variable atmospheric circulation plays an important role in regional climate change, and the occurrence of various extreme events is often accompanied by certain abnormal circulation [14]. Yan et al. [15] compared the trends of extreme temperatures between Europe and China and explained some of these trends by changes in geostrophic wind circulation. The Lamb–Jenkinson (L–J) circulation type classification method combines subjective analysis with objective analysis by defining a circulation index and classification standard that is simple to calculate with meaningful synoptic meteorology [16,17]. Zhu et al. [18] used the Lamb–Jenkinson circulation type classification system and NCEP daily mean sea-level pressure (MSLP) reanalysis data to obtain six circulation indices and a

corresponding 27 circulation types for 16 sub-regions in China. Brisson et al. [19] classified the atmospheric circulation types in Serbia through this method and discussed the frequency changes of different circulation types in spring and autumn and their relationship with precipitation. Teng et al. [20] used this method to study the relationship between summer precipitation and atmospheric circulation in Shandong Province in eastern China. It has been demonstrated that the L–J circulation type classification method is efficient for different regional studies. In Greece, Maheras et al. [21,22] explored the relationship between changes in extreme temperature and atmospheric circulation types in Greece. The results revealed the increase in the frequency of anticyclonic types could explain the upward trend of maximum temperature in summer. In contrast, the trend of decreasing minimum temperature in winter, especially in central and southwestern Greece, characterised by trends of decreasing positive and negative anomalies for most circulation types, cannot be interpreted only by changes in circulation-type frequency. Kolios [12] found a negative correlation of both frequencies of extremely high and low temperatures in Greece with the North Atlantic Oscillation (NAO) monthly index series, which revealed which mode of NAO could enhance the frequency of occurrence of temperature extremes in Greece.

In short, it is beneficial to comparatively assess the variation characteristics of extreme temperature and precipitation events in China and Greece based on updated long-term homogenized daily observations and to explore possible mechanisms for the changing climate extremes in the two regions. In the present paper, we first comparatively demonstrate the temporal and spatial variation characteristics of climate extremes (such as extreme high temperature, extreme low temperature and heavy rainfall) since 1960 in the two countries, based on a set of updated homogenized daily temperature and precipitation time series. Second, we apply a multiple linear regression (MLR) model and MSLP reanalysis data to reveal the relationships between extreme climate indices and the main atmospheric circulation types. The multiple correlation coefficient (R) and coefficient of determination (R^2) are used to assess the predictive power of the regression model. The significance of R is tested by the F-test and the regression coefficients are tested by the t-test at the 0.05 significance level. Section 2 describes the data and methods used. Section 3 demonstrates the temporal and spatial variation characteristics of extreme temperature and precipitation in China and Greece in recent decades. In the same section some typical relationships between extreme climate indices and large-scale atmospheric circulation types in the two countries are also presented. We summarise the main findings and discuss them in Section 4

2. Data and Methods

2.1. Data

2.1.1. Observations

Raw daily maximum temperature (TX), minimum temperature (TN), mean temperature (TG) and precipitation (RR) data records for the period 1960–2021 at 366 stations in China were collected from the China Meteorological Administration, and for the period 1960–2010 at 56 stations in Greece were provided by the Hellenic National Meteorological Service. In this study, we applied the homogenised daily datasets that were produced via a combination of different methods including MASH [23] and Climatol [24]. The MASH method was developed by the Hungarian Meteorological Service. This is a relative homogeneity test procedure based on multiple mutual comparisons between climatically similar series and does not assume a homogenized reference series. The time step of comparisons may be annual, seasonal, or monthly. For the given significance level, the test statistic can be compared to the critical value α (by a Monte Carlo method) and in case of homogeneity it should be smaller. In the Climatol package, original data are normalized using proportions (ratios) or differences depending on the climatological variable. Proportions to normal climatological values are appropriate for zero-limited meteorological

parameters with L-shaped probability distributions (e.g., precipitation), while differences to normal are most suited to normally distributed variables (e.g., temperature). After estimating, all the data, for every original series a series of anomalies (differences between the normalized original and estimated data) are calculated. For shifts in the mean, the standard normal homogeneity test [24] is applied. The details of the recently developed datasets and homogenisation processing are described in [25]. Figure 1 shows the geographical distribution of the Chinese (a) and Greek (b) meteorological stations used in this study.

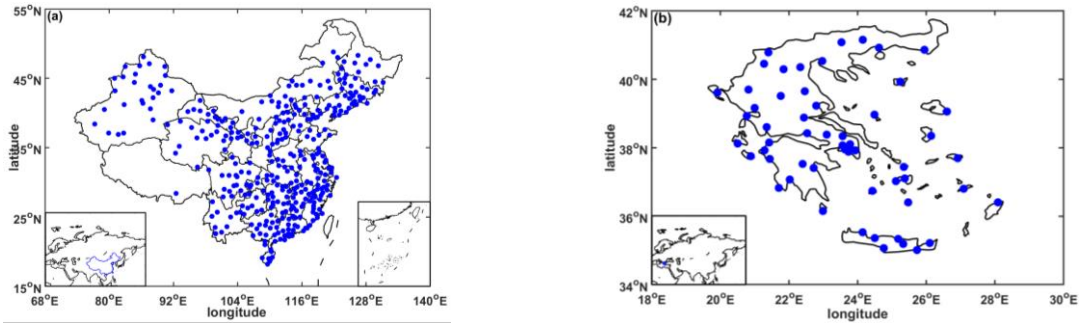

Figure 1. Geographical distribution of the 366 Chinese (**a**) and the 56 Greek (**b**) stations used for calculating extreme climate index time series. Blue dots show the position of the meteorological stations.

2.1.2. Reanalysis Data

Gridded monthly MSLP obtained from the ERA-40 [26] and ERA-5 [27] reanalysis datasets of the European Centre for Medium-Range Weather Forecasts (ECMWF) were used to investigate possible links between large-scale circulation patterns and the regional changes of climate extremes. These reanalyses are available at the relatively high spatial resolution (0.25 ° × 0.25 °) required by the L–J classification method.

2.2. Methods

2.2.1. Calculation of Climate Indices

Based on the homogenized daily temperature and precipitation series, 26 climate indices (Table 1) defined by ETCCDI at each station in China and Greece since 1960 were calculated by using RClimDex (https://github.com/ECCC-CDAS/RClimDex, accessed December 5th, 2021). The base period 1961–1990 was selected for calculating TN10p, TX10p, TN90p, TX90p, R95p and R99p.

In order to investigate the spatial variation of extreme climate indices, the anomalous temperature and precipitation index series (deviation from the mean climatology of the base period 1961–1990) at each station were subjected and then interpolated into 0.5 ° (latitude) × 0.5 ° (longitude) grid data by using the Cressman method and were then used to produce the spatial distribution map of extreme climate index anomalies. The Cressman interpolation algorithm is an objective analysis method [28] that has been widely applied with reasonable accuracy for regional climate analyses.

Table 1. Climate indices defined by ETCCDI.

Climate Index	Indicator Name	Definitions	Units
TXx	Max Tmax	Annual maximum value of daily maximum temperature	°C
TNx	Max Tmin	Annual maximum value of daily minimum temperature	°C
TXn	Min Tmax	Annual minimum value of daily maximum temperature	°C
TNn	Min Tmin	Annual minimum value of daily maximum temperature	°C
TN10p	Cool nights	Percentage of days when TN < 10th percentile	%
TX10p	Cool days	Percentage of days when TX < 10th percentile	%
TN90p	Warm nights	Percentage of days when TN > 90th percentile	%
TX90p	Warm days	Percentage of days when TX > 90th percentile	%
FD0	Frost days	Annual count when TN < 0 °C	Days
SU25	Summer days	Annual count when TX > 25 °C	Days
ID0	Ice days	Annual count when TX < 0 °C	Days
TR20	Tropical nights	Annual count when TN > 20 °C	Days
WSDI	Warm spell duration indicator	Annual count of days with at least 6 consecutive days when TX > 90th percentile	Days
CSDI	Cold spell duration indicator	Annual count of days with at least 6 consecutive days when TN < 10th percentile	Days
GSL	Growing season length	Annual (1st January to 31st December in NH, 1st July to 30th June in SH) count between first span of at least 6 days with TG > 5 °C and first span after July 1 (January 1 in SH) of 6 days with TG < 5 °C	Days
DTR	Daily temperature range	Monthly mean difference between TX and TN	°C
R10MM	Number of heavy precipitation days	Annual count of days when RR >= 10 mm	Days
R20MM	Number of very heavy precipitation days	Annual count of days when RR >= 20 mm	Days
RX5day	Max 5-day precipitation	Annual maximum consecutive 5-day precipitation	mm
RX1day	Max 1-day precipitation	Annual maximum 1-day precipitation	mm
SDII	Simple daily intensity index	Annual total precipitation divided by the number of wet days (RR >= 1mm) in the year	mm/day
CDD	Consecutive dry days	Maximum number of consecutive days with RR < 1 mm	Days
CWD	Consecutive wet days	Maximum number of consecutive days with RR < 1 mm	Days
R95p	Very wet days	Annual total precipitation when RR > 95th percentile	mm
R99p	Extremely wet days	Annual total precipitation when RR > 99th percentile	mm
PRCPTOT	Annual total wet-day precipitation	Annual total precipitation in wet days (RR > 1 mm)	mm

2.2.2. Trend Estimation Method

The Mann–Kendall (MK) test [29,30] and the Theil–Sen estimator [31,32] are two non-parametric tests for time series trends often used by researchers in studying hydrological and climate time series. The Theil–Sen estimator is more effective than the regression equation [33]. In the present study, the Mann–Kendall test was applied at the 0.05 significance level for all extreme index series of China and Greece, to determine the existence of an increasing or a decreasing trend. The Theil–Sen estimator is employed to assess the trend magnitude.

2.2.3. Lamb–Jenkinson Circulation Type Classification System

The Lamb–Jenkinson (L-J) circulation type classification system is an objective and automatic method that reveals the type of atmospheric circulation in an area of interest, based upon MSLP [16,17]. It facilitates objectively quantifying local circulation and assessing its relationship with local climate change from the perspective of synoptic climatology. The basic idea of this method is, based on geostrophic circulation theory, to calculate six circulation indices (u, v, V, ξu, ξv and ξ) with MLSP at 16 gridded points covering the target region (as shown in Figure 2), and then to define the classified atmospheric circulation types for the region based on these indices [34]. The six indices are calculated as follows:

$$u = \frac{1}{2}[P(12) + P(13) - P(4) - P(5)] \quad (1)$$

$$v = \frac{1}{\cos\alpha} \times \frac{1}{4}[P(5) + 2P(9) + P(13) - P(4) - 2P(8) - P(12)] \quad (2)$$

$$V = \sqrt{u^2 + v^2} \quad (3)$$

$$\xi_u = \frac{\sin\alpha}{\sin\alpha 1} \times \frac{1}{2}[P(15) + P(16) - P(8) - P(9)] - \frac{\sin\alpha}{\sin\alpha 2} \times \frac{1}{2}[P(8) + P(9) - P(1) - P(2) \quad (4)$$

$$\xi_v = \frac{1}{2\cos_\alpha^2} \times \frac{1}{4}[P(6) + 2P(10) + P(14) - P(5) - 2P(9) - P(13) + P(3) + 2P(7) + P(11) - P(4) - 2P(8) - P(12) \quad (5)$$

$$\xi = \xi_u + \xi_v \quad (6)$$

P(n) denotes the MSLP at grid point n, u and v the westerly (zonal) and southerly (meridional) components of the geostrophic wind, V the combined wind speed, ξ_u (meridional gradient of u) and ξ_v (zonal gradient of v) the westerly and southerly shear vorticity and ξ the total shear vorticity. α, α_1 and α_2 are the latitudes of C, A_1 and A_2 point, respectively. Once u and v are known, the wind direction can be determined. There are basically two main categories of circulation types. The so-called directional flow type (north: N; northeast: NE; east: E; southeast: SE; south: S; southwest: SW; west: W; northwest: NW) is characterized by the wind direction ($|\xi| < V$). The other category emphasizes rotation of the atmosphere ($|\xi| \geq 2V$), which can either be cyclonic (C) or anticyclonic (A). There is also a hybrid category ($V < |\xi| < 2V$), which can be any combination of the two main categories. In cases where $V < 6$ and $|\xi| < 6$, the circulation is unclassified (UD). In total, there are 27 circulation types. For a given region, it is usually convenient to analyse a few of the most frequent circulation types.

In the present study, using the monthly MSLP reanalysis data in ERA-40 (1960–1978) and ERA-5 (1979–2021), 27 atmospheric circulation types (Table 2) were derived via 16 points to describe circulation features over China (68 °E to 140 °E, 15 °N to 55 °N) and Greece (18 °E to 30 °E, 34 °N to 42 °N), centred at 104 °E, 35 °N and 24 °E, 38 °N, respectively (Figure 2). Six indices had units of hPa per 10 latitudes for China and hPa per 2 latitudes for Greece. The monthly frequencies of circulation types over the two countries were computed and analysed.

Table 2. Lamb–Jenkinson circulation classification types.

$\|\xi\| \le V$	$\|\xi\| \ge 2V$	$V < \|\xi\| < 2V$	$V < 6$ and $\|\xi\| < 6$
N; NE; E; SE; S; SW; W; NW	A; C	CN; CNE; CE; CSECS; CSW; CW; CNW; AN; ANE; AE; ASE; AS; ASW; AW; ANW	UD

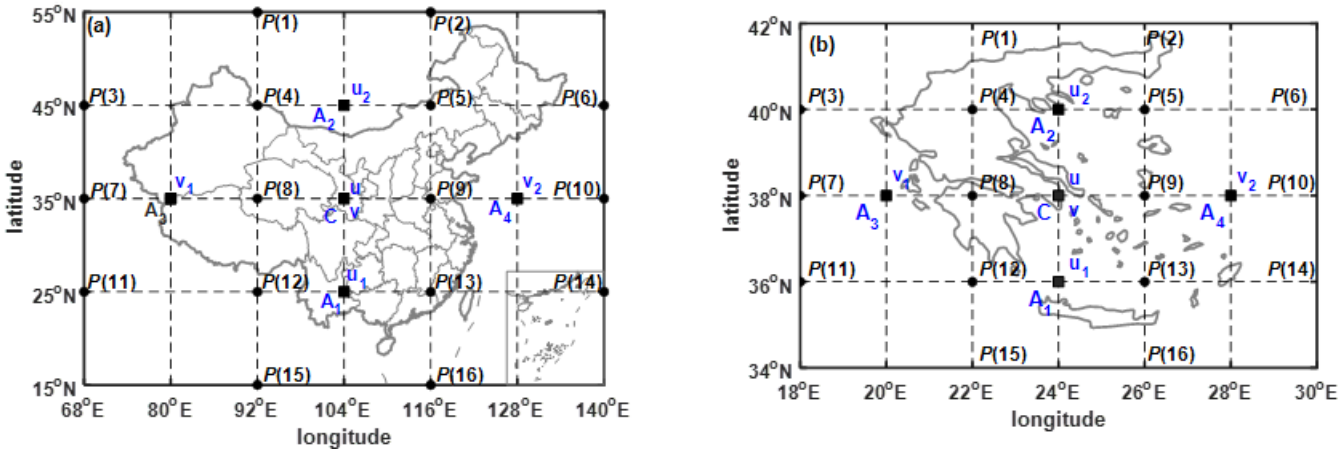

Figure 2. Map showing the 16 grid points used in constructing the circulation climatology in China (**a**) and Greece (**b**).

2.2.4. Multiple Linear Regression

Multiple linear regression models were developed for each station using the frequencies of atmospheric circulation patterns as predictors (independent variables), and the extreme index as the predicted variable (dependent variable). The equation is as follows:

$$\hat{y} = b_0 + b_1 x_1 + b_2 x_2 + \cdots + b_p x_p + \varepsilon \quad (7)$$

where $\hat{y}$ is the predicted variable, x_1 through x_p are p predictors, b_0 is the intercept and b_1 through b_p are the estimated regression coefficients and ε is the random error. Tošić et al. [35] used a MLR model to evaluate the relationship between extreme temperature events and atmospheric circulation and predicted the extreme temperature events in Serbia, suggesting that this model gave the best results for TX90p, FD0 and TN10 in winter.

3. Results

3.1. Comparison of Temporal Variation in Climate Extreme Indices since 1960

3.1.1. Statistics of Estimated Trends since 1960 at all Stations

Figure 3 provides an overview of positive and negative Theil–Sen trends of all indices at 366 stations between 1960 and 2021 in China and at 56 stations between 1960 and 2010 in Greece; Figure 4 shows the corresponding percentage of stations with significant trends according to the MK test. As shown in Figures 4a and 3a, the positive trends prevailed at over 80% of stations of the TXx, TNx, TXn, TNn, TN90p, TX90p, SU25 and TR20 series (up to 100% for TN90p) and most indices related to extreme high temperature (TNx, TN90p, TX90p, SU25 and TR20) were statistically significant in over 80% of stations in China. Correspondingly, the Theil–Sen trends of TN10p, TX10p and FD0 (related to extreme low

temperature) are negative at over 80% of stations (up to 100% for TN10p) and all of them were significant trends. In short, there is good consistency of trends of temperature-based indices across the whole of China. The spatial consistency of trends in precipitation-based indices is relatively weak; only over 60% of stations showed negative trends in RX5day, RX1day, R95 and PRCPTOT. All the precipitation-based indices present significant trends at a limited number of stations (<20%).

In Greece, as seen in Figure 3b, the indices TXx, TNx, TNn, TN90p, SU25 and TR20 presented a positive trend for over forty percent of all stations. In contrast, the indices PRCPTOT and TN10p presented negative trends at over 20% of stations. For each index, however, the statistically significant trends were consistently positive (or negative) across all the corresponding stations (Figure 4b). For example, TXn, TR20, TN90p, and PRCPTOT and TN10p have only negative trends, while TXx, TNx, TXn, WSDI, CDD and R99PTOT have only positive trends. Among the mixed situations (Figure 4b), in some cases a positive (e.g., for TNn, SU25, SDII, R95PTOT) trend prevailed while in the rest of the cases a negative trend (such as for DTR, R10MM and TX10p) prevailed.

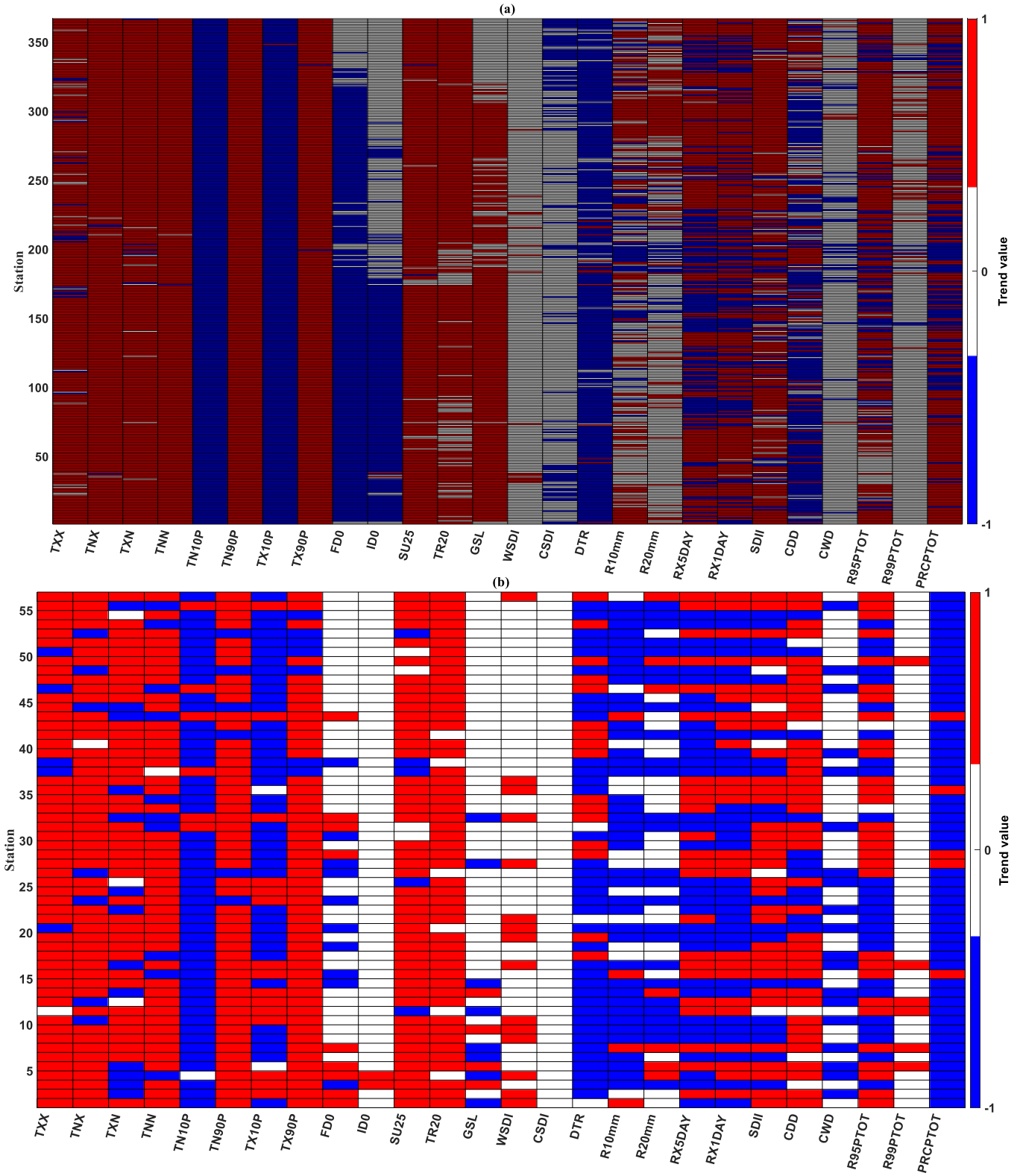

Figure 3. Positive (red) and negative (blue) Theil–Sen trend per station and per climate index between 1960 and 2021 in China (**a**) and between 1960 and 2010 in Greece (**b**). Positive and negative trends on the colour bar are denoted with '1' and '-1', respectively; zero trends are denoted with '0'.

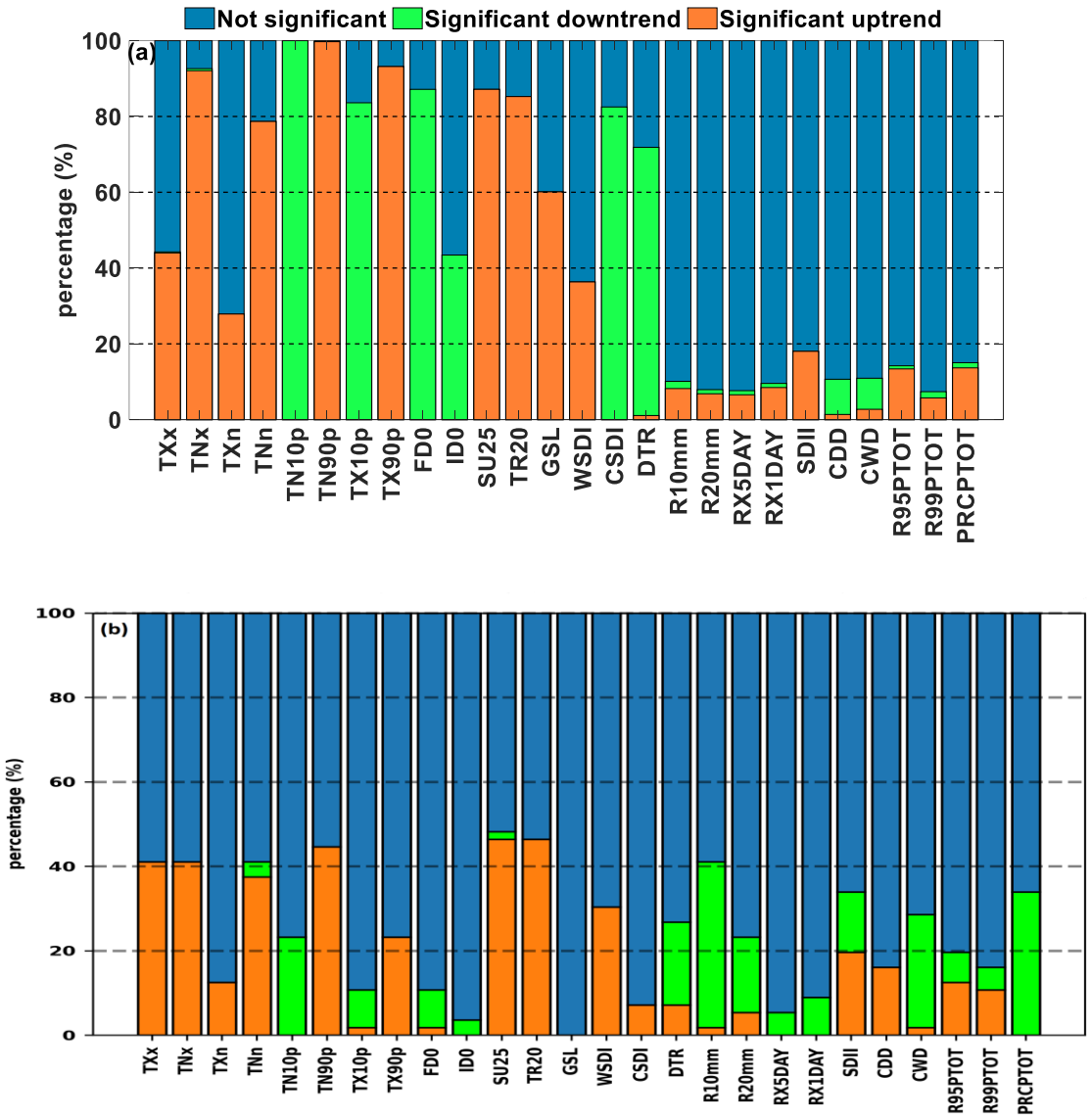

Figure 4. Climate indices and corresponding percentage of stations with significant trends between 1960 and 2021 in China (**a**) and between 1960 and 2010 in Greece (**b**) according to the MK test.

3.1.2. Comparison of Temporal Variation Characteristics of Regional Mean Climate Extreme Index Series between 1960 and 2010

Figure 5 quantitatively describes the temporal variation characteristics of regional mean annual extreme index series between 1960 and 2021 in China and between 1960 and 2010 in Greece. Table 3 gives their slopes estimated by the Theil–Sen estimator and corresponding significance by the MK test since 1960. Limited by the availability of data in Greece, in this section, we just compared and analysed the results in the two countries during the same period, i.e., 1960–2010.

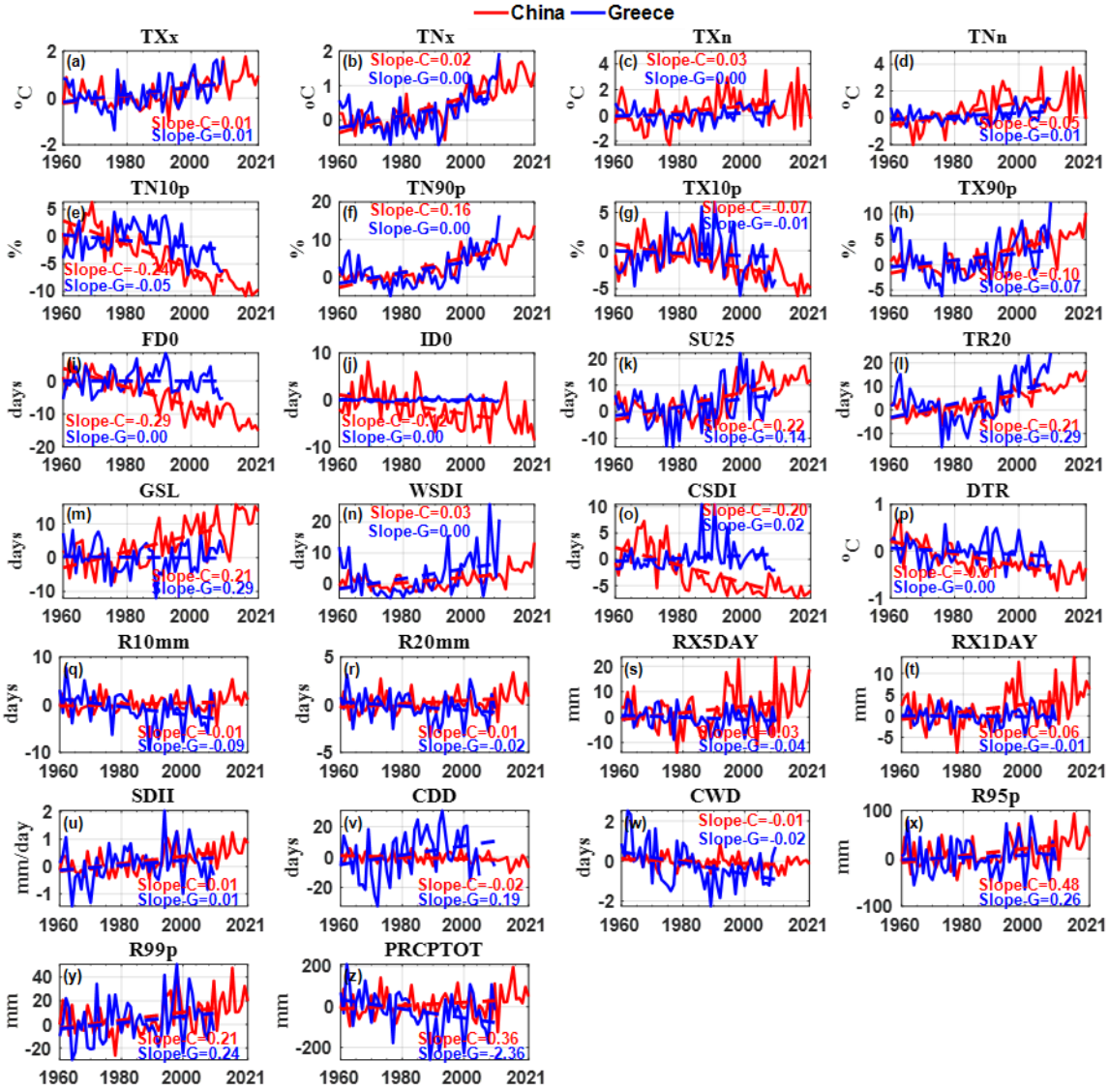

Figure 5. Extreme temperature (**a**–**p**) and precipitation (**q**–**z**) index series in China and Greece and their estimated slopes (unit: y-axis unit per year) during the same period 1960–2010.

Regarding the temperature-based indices, the regional mean TN10p, TX10p, FD0, ID0, CSDI and DTR showed significant downward trends with different degrees, while other indices showed upward trends between 1960 and 2010 in China. Specifically, the series of TXx, TNx, TXn and TNn showed significant positive trends of 0.1 °C/10a, 0.2 °C/10a, 0.3 °C/10a and 0.5 °C/10a, respectively. TXn and TNn displayed more obvious interannual variability than TXx and TNx, especially after 2010. Meanwhile, the trends of annual minimum temperature (TNn and TNx) were larger than those of annual maximum temperature (TXn and TXx), indicating greater changes of night-time extreme temperature than those of daytime. TN10p and TX10p significantly decreased at the rate of −2.4%/10a and −0.7%/10a, while TN90p and TX90p presented a significant upward trend at a rate of 1.6%/10a and 1.0%/10a, respectively, indicating warm days and nights increased while cool days and nights decreased. FD0 and ID0 decreased significantly but SU25 and TR20 increased significantly, and the changing rates of trends were larger than 2.0 d/10a, except for ID0 (−1.2 d/10a). Negative trends in CSDI (−2.0 d/10a) and DTR (−0.10 d/10a) and positive trends in GSL (2.40d/10a) and WSDI (0.3d/10a) were also observed. Overall, the decreases in FD0, ID0, CSDI and DTR and the increases in SU25, SU20 and WSDI all reflected climatic warming in China against the background of global warming. It is worthwhile noting that the trends of most climate indices (except for R10MM) in

China are more significant between 1960 and 2021 than between 1960 and 2010, implying large changes in the last decade and hence the importance of updating the assessment of climate change.

For Greece, the extreme temperature indices TN10p and TX10p exhibited downward trends at a rate of −0.5%/10a and −0.1%/10a, respectively. TXn, FD0, ID0, WSDI, TNx, TN90p and DTR were with slight trends close to zero. The other indices showed upward trends at different rates, significant in the TXx, TR20 and WSDI regional mean series. Clearly, the upward trends of TXx and TNx were consistent with those in China, with a rate of 0.10 °C/10a and 0.20 °C/10a, but the trends of TXn and TNn were obviously different: close to zero in Greece but up to 0.3 °C/10a and 0.5 °C/10a in China. Compared with China, the magnitudes of the increasing or decreasing trends of TN10p, TX10p, TN90p and TX90p in Greece were smaller, and the TX10p time series had larger interannual variability, showing an upward trend from the middle and late 1970s to the 1990s while showing a downward trend again from the early 21st century. The trend of FD0 and ID0 was close to 0, while significant upward trends of 1.4d/10a and 2.9d/10a were observed in SU25 and TR20, indicating that the extreme temperature had a slight change in the winter half of the year, while it increased significantly in the summer half of the year in Greece. This change characteristic was different from that in China, i.e., increased in all seasons. WSDI had a slight change in the early stages but began to increase significantly after 1990. Except for larger values in the 1990s, the change of CSDI in other time periods was relatively flat. For DTR, the trend was basically 0; however, Maheras et al. (2006) [22] found that TX (TN) had an overall increasing (decreasing) trend between 1958 and 2000 in Greece, revealing a different trend of DTR.

To sum up, extreme cold events tended to decrease while extreme warm events increased both in China and in Greece, which can be partially attributed to global warming. However, the extreme temperature (FD0 and ID0) tended to be warmer in the winter half of the year in China while this was not the case in Greece.

Table 3. Trends of regional mean extreme indices in Greece and China since 1960.

Country	Time Period	TXx	TNx	TXn	TNn	TN10p	TN90p	TX10p
Greece	1960–2010	0.1 *	0.0 *	0.0	0.1	−0.5	0.0 *	−0.1
China	1960–2010	0.1 *	0.2 *	0.3 *	0.5 *	−2.4 *	1.6 *	−0.7 *
China	1960–2021	0.2 *	0.3 *	0.2 *	0.4 *	−2.2 *	2.0 *	−0.9 *
		TX90p	**FD0**	**ID0**	**SU25**	**TR20**	**GSL**	**WSDI**
Greece	1960–2010	0.7	0.0	0.0	1.4	2.9 *	2.9	1.3 *
China	1960–2010	1.0 *	−2.9*	−1.2 *	2.2 *	2.1 *	2.4 *	0.3
China	1960–2021	1.2 *	−2.9*	−1.0 *	2.5 *	2.7 *	2.5 *	0.8 *
		CSDI	**DTR**	**R10MM**	**R20MM**	**RX5day**	**RX1day**	**SDII**
Greece	1960–2010	0.2	0.0	−0.9 *	−0.2	−0.4	−0.1	0.1
China	1960–2010	−2.0 *	−0.1 *	−0.1	0.1	0.3	0.6	0.1 *
China	1960–2021	−1.5 *	−0.1 *	0.2	0.2 *	1.2 *	0.8 *	0.1 *
		CDD	**CWD**	**R95p**	**R99p**	**PRCPTOT**		
Greece	1960–2010	1.9	−0.2 *	2.6	2.4	−23.6 *		
China	1960–2010	−0.2	−0.1 *	4.8	2.1	3.6		
China	1960–2021	−0.5	−0.1 *	7.3 *	3.2 *	8.4 *		

* Trends passing the 0.05 significance level according to the MK test. Unit: same as the unit in Figure 5 but per decade.

Regarding the extreme precipitation indices, Figure 5 and Table 3 show that except for R10MM, CDD and CWD, the regional mean series of R20MM, Rx5day, Rx1day, SDII, R95p, R99p and PRCPTOT showed positive trends of 0.1 mm/10a, 0.3 mm/10a, 0.6 mm/10a, 0.1 mm/10a, 4.8 mm/10a, 2.1 mm/10a and 3.6 mm/10a between 1960 and 2010 in

China, respectively. Among all these indices, only SDII and CWD showed a statistically significant trend between 1960 and 2010. Clearly, the values of RX1day and RX5day in the 1990s were higher than in the other years, revealing obvious interdecadal variability, which makes the long-term trends uncertain. Most of the updated trends between 1960 and 2021 emerge to be significant.

For Greece, the indices SDII, CDD, R95p and R99 showed an increasing trend while not significant between 1960 and 2010. The other six indices, R10MM, R20MM, RX1day, RX5day, CWD and PRCPTOT showed negative trends with rates of −0.9d/10a, −0.2d/10a, −0.4 mm/10a, −0.1 mm/10a, −0.2d/10a and −23.6 mm/10a, respectively, but were statistically significant only for R10MM, CWD and PRCPTOT.

Comparing the trends of precipitation-based indices between the two countries, it is interesting to observe that most indices showed opposite trends; only SDII, CWD, R95p and R99p presented consistent trends. The SDII series showed an increasing trend of 0.1 mm/10a both in China and Greece. CWD exhibited a significant trend of 0.2d/10a in Greece, twice that in China. Both R95p and R99p in the two countries presented a relatively obvious increase, but the increasing rate in the R95p series in China was about twice that of Greece. Among all indices with opposite trends, the largest difference was found in PRCPTOT, which had a sharp decreasing trend of −23.6 mm/10a in Greece but an increasing trend of 3.6 mm/10a in China.

In short, total precipitation (PRCPTOT), extreme precipitation (R20MM, RX5day, RX1day, R95p and R99p) and intensity (SDII) increased, but the persistent rainfall (CWD) and persistent dry days (CDD) decreased to a certain extent between 1960 and 2010 in China. The total precipitation (PRCPTOT) as well as the persistent precipitation (CWD) decreased, while the extreme heavy precipitation (R95p and R99p) and persistent dry days (CDD) showed an increasing trend in Greece.

3.2. Comparison of Geographical Patterns of Climate Extreme Indices between 1960 and 2010

The regional mean trend of extreme temperature and precipitation indices reflects the overall change trend in a region, but due to the differences in natural factors such as sea and land location, altitude and terrain, there are different spatial change characteristics in each region, especially at a local scale. In this section, we just selected the indices with larger different trends in the regional mean series (listed in Table 3) of the two countries to analyse the spatial distribution characteristics of their anomalies. Four temperature indices, FD0, ID0, CSDI and DTR, were mainly related to extreme cold events such as frost and freezing. The four precipitation indices were R20MM, RX5day, CDD and PRCPTOT.

Figure 6 shows the spatial distributions of eight extreme index anomalies between 1960 and 2010 relative to the base period 1961–1990 in China and Greece. For the four chosen precipitation-based indices, different spatial distribution characteristics exist between the two countries, i.e., the increasing trends prevail in R20MM, RX5day and PRCPTOT and the decreasing trends occur in CDD in most parts of China, while the opposite occurs in Greece. There are similar spatial distributions of anomalies except for CDD in China. Positive anomalies of R20MM (Figure 6a1), RX5day (Figure 6b1) and PRCPTOT (Figure 6d1) are observed mainly in Western China, Southeast China, and Northeast China, indicating that the increasing trends prevail in most parts of China. However, negative anomalies for CDD occupy most parts of the country (Figure 6c1) revealing the decreasing trends and positive values are mainly in the south of South China, most parts of Southwest China and the south of North China. For Greece, the spatial distribution patterns of R20MM (Figure 6a2) and RX5day (Figure 6b2) are basically similar, i.e., the anomalies are just positive northwest of the Pindus Mountains. Differing from the situation in China, CDD shows positive anomalies across the whole of Greece, indicating increasing trends (Figure 6c2). The anomalies of PRCPTOT (Figure 6d2) are negative at all stations, indicating that the decreasing trends can be observed almost anywhere.

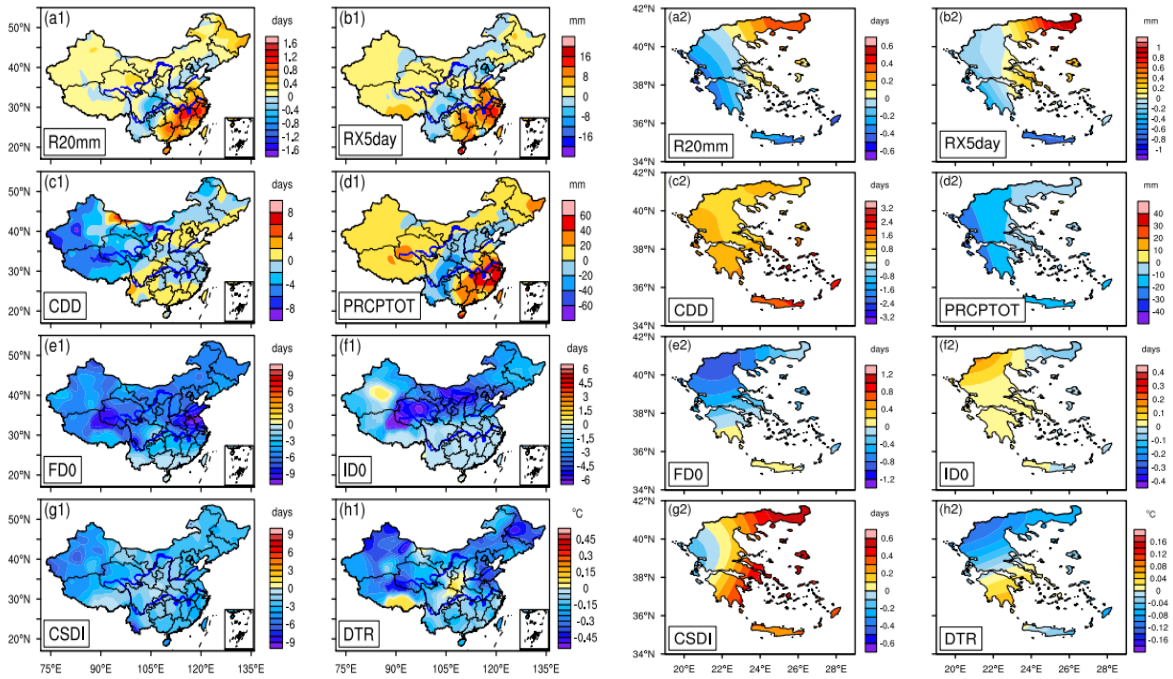

Figure 6. The spatial distribution of extreme climate index anomalies between 1960 and 2010 in China (**a1**–**h1**) and Greece (**a2**–**h2**). Anomalies are differences from average conditions in the 1961 - 1990 period.

For extreme temperature indices, obviously, FD0 (Figure 6e1) and CSDI (Figure 6g1) anomalies were negative throughout China, revealing that they decreased from the reference period to recent decades. The negative anomalies also occurred in most of China except for a small part of central Xinjiang for ID0 (Figure 6f1), and except for southwest Tibet and most of Shaanxi Province for DTR (Figure 6h1). The trend of the regional mean FD0 index in Greece tended to 0 (Table 3), but looking at its spatial distribution of anomalies, they were positive only in Crete and the southern part of Crete and the southern region of Peloponnese (Figure 6e2). It is observed that the regional average trend cannot accurately represent the climate situation at the local scale. The spatial distribution of anomalies in ID0 (Figure 6f2) and CSDI (Figure 6g2) demonstrates that extreme cold events tended to increase in whole country except for a small area. DTR showed an increasing trend in most areas in the southeast of the Pindus Mountains.

3.3. Relationship between Climate Extremes and Circulation Types

3.3.1. Main Circulation Types in China and Greece

According to the L–J objective circulation classification system, we defined 27 different circulation types at a monthly scale over the study period. There were eight pure directional types defined by the wind direction (N, NE, E, SE, S, SW, W and NW), two pure types controlled by the strength of the geostrophic vorticity (C and A), sixteen hybrid types (eight cyclonic and eight anticyclonic for each direction). Hybrid types are a mixture of direct and vorticity types (C or A). The difference between the pure directional types and the hybrids is in the strength of the flow.

Figure 7 gives the main circulation types and their corresponding frequencies covering the period of 1960 - 2021 in China and 1960–2010 in Greece. From the perspective of the whole period, the anticyclonic (including mixed anticyclonic) circulation in China was far more than the cyclonic circulation, dominated by A (20.16%), AE (17.34%), SE (16.53%), ASE (9.81%), N (7.80%), NE (7.80%), ANE (7.39%), S (6.72%) and E (3.09%), totally accounting for 96.64% of all circulation types, and the other circulation types accounting for less than 4%. In contrast, the cyclonic circulation and cyclonic mixed circulation types

were in the majority in Greece. The main types were NE (32.52%), N (24.51%), C (8.66%), S (7.84%), SE (7.19%), E (6.70%), CN (4.90%), CE (1.96%), CSE (1.80%) and CN (1.14%), accounting for 97.22% of all circulation types and each of the remaining types accounts for a small proportion (<1%).

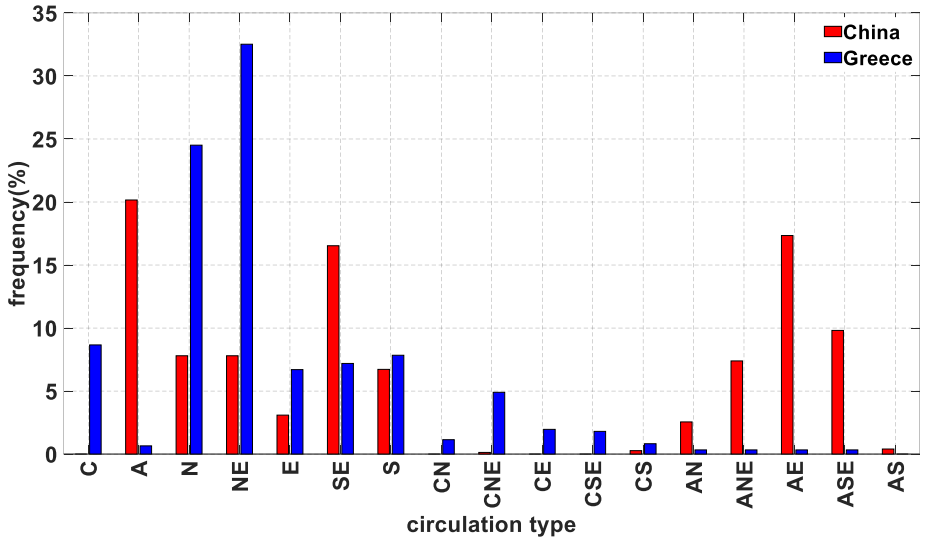

Figure 7. Main circulation types and their corresponding frequencies covering the period of 1960 - 2021 in eastern China and 1960–2010 in Greece.

3.3.2. Main Circulation Types in China and Greece

Multiple linear regression models were applied to find the relationship between extreme indices and atmospheric circulation types. Eight circulation types in China (A, N, NE, SE, S, ANE, AE and ASE) and six in Greece (C, N, NE, E, SE and S), which account for a large proportion (each accounting for more than 5%) of all circulation types, were considered as predictor variables. Eight climate indices (R20MM, RX5day, CDD, PRCPTOT, FD0, ID0, CSDI and WSDI) with obvious differences in trends between the two countries were used as predicted variables

Table 4 shows the multiple correlation coefficients of MLR models for eight climate indices in China and Greece. For China, the correlation between extreme indices and main circulation types between 1960 and 2021 indicates that the strongest relationship existed in RX5day and WSDI, with a correlation coefficient higher than 0.53. However, there are no significant correlations for the other six indices. For Greece, the highest correlation values were 0.71 for R20MM, 0.61 for RX5day, 0.50 for CDD, 0.74 for PRCPTOT and 0.57 for FD0, which were significant at the 0.05 significance level, respectively. Compared with China, there is a better correlation between climate indices and circulation types in Greece, especially for extreme precipitation indices. To some extent, these MLR models describe whether circulation types have obvious influences on the trends of certain climate indices in China and Greece.

Table 4. Results from MLR models for eight climate indices since 1960 in China and Greece.

	R20MM	RX5day	CDD	PRCPTOT	FD0	ID0	WSDI	CSDI
China	0.35	0.53 *	0.23	0.35	0.38	0.49	0.54 *	0.35
Greece	0.71 *	0.61 *	0.50 *	0.74 *	0.57 *	0.10	0.27	0.18

* The multiple correlation coefficient passing the 0.05 significance level according to the F test.

Having established the regression models, we attempted to infer the influences of circulation types on climate indices in China and Greece based on the corresponding regression coefficients. For instance, in China, the N-type circulation accounts for 26.34% of

all types, which has a significant correlation with PRCPTOT, RX5days and WSDI. Note that most of the annual precipitation in China occurs in summer, while the N-type circulation pattern is also mainly observed in summer. According to Figure 8a, the N-type corresponds to southerly winds along the eastern coast of China, with low pressure centres over most of eastern China. This circulation pattern in summer favours higher than usual warm and humid air currents from the low latitudes in eastern China and enhances precipitation indices such as RX5day and PRCPTOT and temperature indices such as WSDI. In contrast, such a circulation pattern does not favour the drought index (CDD). As shown in Figure 8b, the N-type frequency series has an increasing trend (0.08 times/10a) between 1960 and 2021, while RX5day and WSDI have positive trends of 1.2 mm/10a and 0.8 d/10a, respectively, and the CDD has a decreasing trend of −0.5 d/10a (Figure 8b and Table 3).

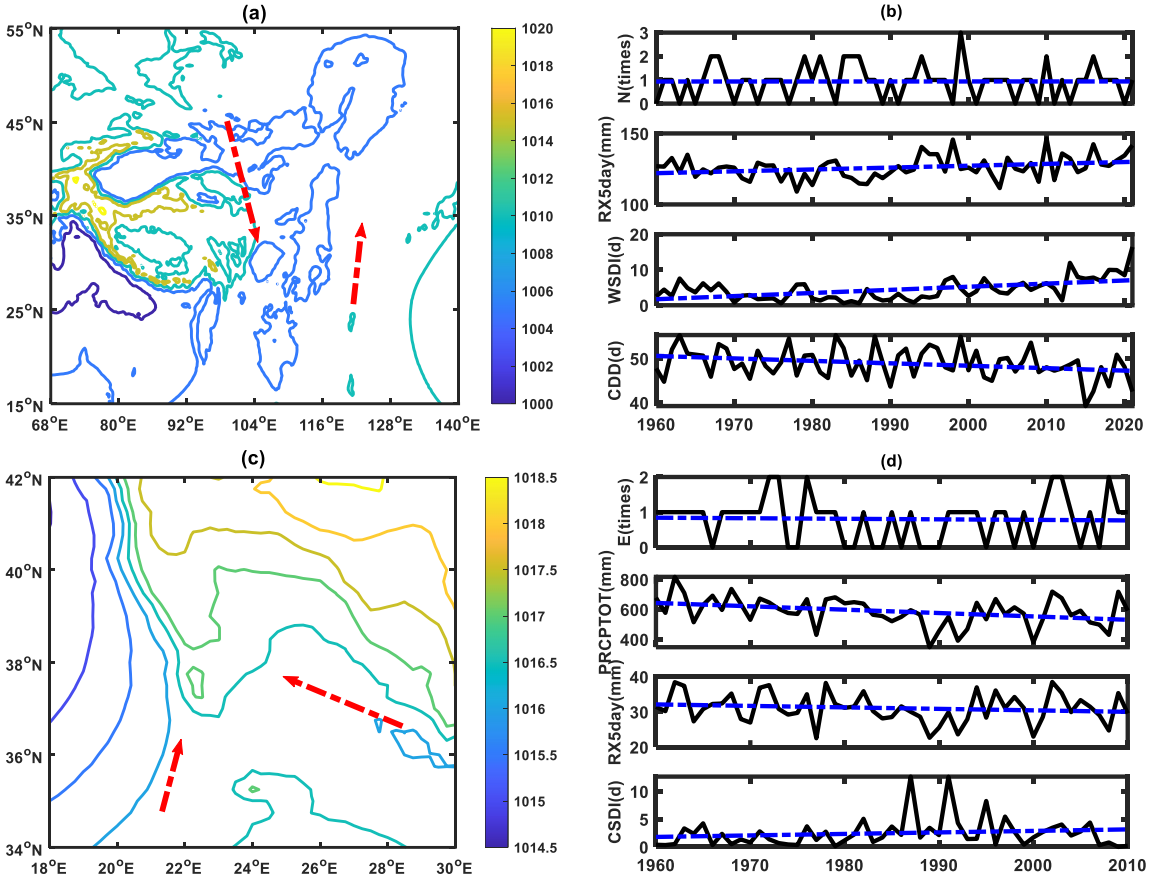

Figure 8. The mean MLSP field of N-type over China (**a**) and E-type over Greece (**c**) (Unit: hpa) and their annual frequency series compared with sample climate index series since 1960 (**b** and **d**). Broken red arrows show the prevailing wind directions.

In Greece, we showed a striking decreasing trend in PRCPTOT (−15.82 mm/10a) in winter. Since the rainy season in Greece is mainly winter, we found a relatively frequent circulation pattern, the E-type, which only occurs in the winter half of the year (November–April) and significantly influences RX5day, CDD and PRCPTOT. As shown in Figure 8c, the E-type induces easterly winds across the eastern boundary of the region together with some southerly winds from the southwest. Such a circulation pattern tends to induce cyclonic disturbances in the dominant winter westerlies over Greece, favourable for local precipitation and warm temperatures. In fact, the E-type frequency series has a negative trend of −0.02 times/10a, while PRCPTOT and RX5day decrease by −23.6 mm/10a and −0.4 mm/10a, respectively, and CSDI has an increasing trend of 0.2d/10a between 1960 and 2010 (Figure 8d).

The above two regional cases demonstrate quite well the relationship between large-scale atmospheric circulation types and regional climate extremes. The changes in large scale circulation types, coherent with the regional climate trends, help to confirm the results of the present study.

4. Summary and Conclusions

Based on the homogenized daily temperature and precipitation data (1960 - 2021 for China and 1960 - 2010 for Greece), this paper demonstrated the spatial and temporal variations of 26 extreme temperature and precipitation indices in China and Greece and their association with the main atmospheric circulation types during the past several decades. The main results are summarized as follows.

The long-term temporal variation of climate extreme indices during the same period 1960 - 2010 in China and Greece exhibits different characteristics. In China, extreme cold events (TN10p, TX10p, FD0, ID0 and CSDI) decreased, but extreme warm events (TXx, TNx, TXn, TNn, TN90p, TX90p, SU25, TR20 and WSDI) increased. The total precipitation (PRCPTOT), extreme precipitation (R20MM, RX5day, RX1day, R95p and R99p) and intensity (SDII) increased, but persistent rainfall (CWD) and persistent dry days (CDD) decreased to a certain extent. In Greece, total precipitation as well as persistent precipitation decreased, while extreme heavy precipitation (R95p and R99p) and persistent dry days (CDD) exhibited an increasing trend. Extreme cold events decreased while extreme warm events increased and the trend magnitudes in cold nights and warm nights were greater than those in cold days and warm days in both countries, which is consistent with the background of global warming. However, extreme temperatures (FD0 and ID0) became warmer in the winter half of the year in China but their respective trend in Greece is small.

From the spatial distribution of extreme climate index anomalies, it can be seen that CDD increased in most of Southwest China and the south of North China, while PRCPTOT decreased and temperatures increased, resulting in an increasing probability of extreme weather conditions such as droughts in these regions. In contrast, CDD showed negative trends in Northwest China and the Qinghai–Tibet Plateau. R20MM, PRCPTOT and RX5day increased on the southeast coast, indicating the increasing probability of extreme precipitation. The decreasing trends of four extreme temperature indices (FD0, ID0, CSDI and DTR) prevailed across China. In comparison, CDD increased in most of Greece, while PRCPTOT significantly decreased. R20MM and RX5day revealed similar geographical patterns, with decreasing trends in most of Greece (except for the northwest of the Pindus Mountains), indicating the increasing probability of droughts. The southeast and northwest sides of the Pindus Mountains belong to different climate zones and the precipitation on the northwest side of the mountains is higher than that on the southeast side. In comparison, the frequency of extreme precipitation events increased. The extreme cold events in Greece showed a decreasing trend.

Multiple linear regression modelling was used to investigate the relationship between large-scale circulation types and climate indices in the two countries. Eight/six circulation types with higher frequencies, which accounted for more than 5% of the total, were used as predictors for China/Greece and the regional climate indices as the predicted variable. The results showed a significant correlation ($p < 0.05$) for RX5day and WSDI in China and for R20MM, RX5day, CDD, PRCPTOT and FD0 in Greece, respectively. Compared to China, there was a better correlation between extreme climate indices and circulation types in Greece, especially for the extreme precipitation indices. This is partly because the circulation types were calculated for a very large area over China, including the Qinghai–Tibet Plateau, where the MSLP field bears large biases [15]. In general, the circulation types calculated over such large areas should be used with caution. Nevertheless, the coherent changes between most of the regional climate indices and corresponding circulation types indicate that further investigation of underlying mechanisms of the different regional climate variations is required, especially dealing with climate-sensitive regions such as the Tibetan Plateau [36]. High-resolution regional climate modelling with a

focus on climate extremes has emerged in recent years [37–39], which also paves the way towards further comparative studies of the observed changes of climate extremes revealed in the present study.

Author Contributions: Conceptualization, A.A.A. and Z.Y.; methodology, A.A.A., Z.Y.; software, P.I., L.Z.; formal analysis, L.Z., Z.Y., P.I., A.A.A., A.M., Y.S.; investigation, L.Z., Z.Y., A.A.A., P.I., A.M.; resources, A.M.; data curation, A.A.A., Z.Y.; writing—original draft preparation, L.Z., P.I.; writing—review and editing, Z.Y., A.A.A., A.M.; visualization, L.Z., P.I.; supervision, Z.Y., A.A.A.; project administration, Z.Y., A.A.A.; funding acquisition, Z.Y., A.A.A. All authors have read and agreed to the published version of the manuscript

Funding: This work was funded by National Key Technologies Research and Development Program 'Comparative study of changing climate extremes between China and Europe/Greece based on homogenized daily observations' (Grant No. 2017YFE0133600) and the Hellenic and Chinese Governments, in the frame of the Greek–Chinese R and T Cooperation Programme project "Comparative study of extreme climate indices in China and Europe/Greece, based on homogenised daily observations—CLIMEX" (Contract T7ΔKI-00046).

Institutional Review Board Statement: Not applicable.

Informed Consent Statement: Not applicable.

Data Availability Statement: Data can be provided after request to the corresponding authors.

Acknowledgments: The ERA-40 data for the period 1960–1978 were downloaded from https://apps.ecmwf.int/datasets/data/era40-moda/levtype=sfc/ and the ERA-5 data for the period 1979–2021,from https://cds.climate.copernicus.eu/cdsapp#!/dataset/reanalysis-era5-single-levels-monthly-means?tab=form

Conflicts of Interest: The authors declare no conflicts of interest.

References

1. IPCC. 2021: Summary for Policymakers. In *Climate Change 2021: The Physical Science Basis. Contribution of Working Group I to the Sixth Assessment Report of the Intergovernmental Panel on Climate Change*; Cambridge University Press: Cambridge, UK, 2021; *in press*.
2. Yan, Z.; Ding, Y.; Zhai, P.; Song, L.; Cao, L.; Li, Z. Re-assessing climatic warming in China since 1900. *J. Meteor. Res.* **2020**, *34*, 243–251. https://doi.org/10.1007/13351-020-9839-6.
3. Yao, T.; Bolch, T.; Chen, D.; Gao, J.; Immerzeel, W.; Piao, S.; Su, F.; Thompson, L.; Wada, Y.; Wand, L.; et al. The imbalance of the Asian water tower. *Nat. Rev. Earth. Environ.* **2022**, *3*, 618–632. https://doi.org/10.1038/s43017-022-00299-4.
4. Ren, G.; Feng, Guo.; Yan. Z. Progresses in observation studies of climate extremes and changes in mainland China. Climatic. Environ. Res. **2010**, *15*, 337–353. (In Chinese)
5. Shi, J.; Cui, Lin.; Ma, Y.; Du, H.; Wen, K. Trends in temperature extremes and their association with circulation patterns in China during 1961–2015. *Atmos. Res.* **2018**, *212*, 259–272. https://doi.org/10.1016/j.atmosres.2018.05.024.
6. Yin, H.; Sun, Y. Characteristics of extreme temperature and precipitation in China in 2017 based on ETCCDI indices. *Adv. Climate. Chang. Res.* **2019**, *15*, 363–373. (In Chinese)
7. Wang, J.; Yan, Z. Rapid rises in the magnitude and risk of extreme regional heat wave events in China. *Weather. Clim. Extrem.* **2021**, *34*, 100379. https://doi.org/10.1016/j.wace.2021.100379.
8. Lin, P.; He, Z.; Du, J.; Chen, L.; Zhu, X.; Li, J. Recent changes in daily climate extremes in an arid mountain region, a case study in northwestern China's Qilian Mountains. *Sci. Rep.* **2017**, *7*, 2245. https://doi.org/10.1038/ s41598-017-02345-4.
9. Li, X.; You, Q.; Ren, G.; Wang, S.; Zhang, Q.; Yang, J.; Zheng, G. Concurrent droughts and hot extremes in Northwest China from 1961 to 2017. *Int. J. Climatol.* **2019**, *39*, 2186–2196. https://doi.org/10.1002/joc.5944.
10. Pei, L.; Yan, Z.; Chen, D.; Miao, S. The Contribution of Human-Induced Atmospheric Circulation Changes to the Record-Breaking Winter Precipitation Event over Beijing in February 2020. *Bull. Amer. Meteor. Soc.* **2022**, *103*, S55–S60. https://doi.org/10.1175/BAMS-D-21-0153.1.
11. Bartzokas, A.; Houssos, E.E. Extreme Temperature Events in NW Greece. In Proceedings of the 10th International Conference on Harmonisation within Atmospheric Dispersion Modelling for Regulatory Purposes, Crete, Greece, 2005; pp. 556–560. Available online: https://www.researchgate.net/publication/233898112 (accessed on 1 September 2022).
12. Kolios, S.; Antonatou, G.; Zervas, E. Observed temperature extremes in Greece and their relation with North Atlantic Oscillation. *Int. J. Global. Warm.* **2018**, *15*, 392–412. https://doi.org/10.1504/IJGW.2018.093746.
13. Houssos. E. E.; Bartzokas, A. Extreme precipitation events in NW Greece. *Adv. Geosci.* **2006**, *7*, 91–96. https://doi.org/10.5194/adgeo-7-91-2006.

14. Li, C.; Yang, H.; Zhao, J. Combinational anomalies of atmospheric circulation system and occurrences of extreme weather/climate events. *Trans. Atmos. Sci.* **2019**, *42*, 321–333. https://doi.org/10.13878/j.Cnki.Dqkxxb.20190302001(In Chinese)
15. Yan, Z.; Jones, P.D.; Davies, T.D.; Moberg, A.; Bergstrom, H.; Camuffo, D.; Cocheo, C.; Maugeri, M.; Demaree, G.; Verhoeve, T.; et al. Trends of extreme temperatures in Europe and China based on daily observations. *Clim. Chang.* **2002**, *53*, 355–392. https://doi.org/10.1023/A:1014939413284.
16. Lamb, H.H. Types and spells of weather around the year in the British Isles. *Q. J. R. Meteorol. Soc.* **1950**, *76*, 393–438.
17. Jenkinson, A.; Collison, F. An initial climatology of gales over the North Sea. In *Synoptic Climatology Branch Memorandum*; Meteorological Office: Exeter, UK, 1977; Volume 62, pp. 1–62.
18. Zhu, Y.; Chen, D.; Li, W. Lamb-Jenkinson Circulation Type Classification System and Its Application in China. *J. Nanjing Inst. Meteorol.* **2007**, *30*, 289–297. (In Chinese)
19. Brisson, E.; Demuzere, M.; Kwakernaak, B.; Lipzig, N.P.M. Van. Relations between atmospheric circulation and precipitation in Belgium. *Meteor. Atmos. Phys.* **2011**, *111*, 27–39.
20. Teng., H. Relationship Between Circulation Patterns and Summer Precipitation in Shangdong Province. *J. Arid. Meteor.* **2016**, *34*, 789–795. https://doi.org/10.11755/j.issn.1006-7639(2016)-05-0789 (In Chinese)
21. Maheras, P.; Tolika, K.; Anagnostopoulou, C.; Vafiadis, M.; Patrikas, I.; Flocas, H.A. On the relationships between circulation types and changes in rainfall variability in Greece. *Int. J. Climat.* **2004**, *24*, 1695–1712.
22. Maheras, P.; Flocas, H.A.; Tolika, K.; Anagnostopoulou, K.; Vafiadis, M. Circulation types and extreme temperature changes in Greece. *Clim. Res.* **2006**, *30*, 161–174.
23. Szentimrey, T. Multiple Analysis of Series for Homogenisation (MASH). In Proceedings of the Second Seminar for Homogenisation of Surface Climatological Data. Budapest, Hungary, 9–13 November 1998; WCDMP-No. 41; WMO: Geneva, Switzerland, 1999; pp. 27–46.
24. Guijarro, J.A. Homogenisation of Climatic Series with Climatol—Version 3.1.1. 2021. Available online: https://climatol.eu/homog_climatol-en.pdf (accessed on 4 April 2022).
25. Argiriou, A.A.; Li, Z.; Armaos, V.; Mamara, A.; Shi, Y.; Yan, Z. Homogenized Monthly and Daily Temperature and Precipitation Time Series in China and Greece since 1960. *Adv. Atmos. Sci.* **2022**. (Manuscript under review, with datasets DOIs: 10.57760/sciencedb.01720 for Greece and 10.57760/sciencedb.01731 for China)
26. Uppala, S.M.; KÅllberg, P.W.; Simmons, A.J.; Andrae, U.; Bechtold, V.D.C.; Fiorino, M.; Gibson, J.K.; Haseler, J.; Hernandez, A.; Kelly, G.A.; et al. The ERA-40 re-analysis. *Q. J. R. Meteorol. Soc.* **2005**, *131*, 2961–3012. https://doi.org/10.1256/qj.04.176.
27. Muñoz-Sabater, J.; Dutra, E.; NAgustí-Panareda, A.; Albergel, C.; Arduini, G.; Balsamo, G.; Boussetta, S.; Choulga, M.; Harrigan, S.; Hersbach, H.; et al. ERA5-Land: A state-of-the-art global reanalysis dataset for land applications. *Earth Syst. Sci. Data* **2021**, *13*, 4349–4383. https://doi.org/10.5194/essd-13-4349-2021.
28. Cressman, G.P. An operational objective analysis system. *Mon. Wea. Rev.* **1959**, *87*, 367–374. https://doi.org/10.1175/1520-0493(1959)087<0367: AOOAS>2.0.CO;2.
29. Mann, H.B. Nonparametric tests against trend. *Econometrica* **1945**, *13*, 245–259. https://doi.org/10.2307/1907187.
30. Kendall, M.G. *Rank Correlation Methods*; Oxford University Press: New York, NY, USA, 1975
31. Theil, H. A rank-invariant method of linear and polynomial regression analysis. I, II, III. *Nederl. Akad. Wetensch. Proc.* **1950**, *53*, 386–392, 521–525, 1397–1412.
32. Sen, P. Estimated of the regression coefficient based on Kendall's Tau. *J. Am. Stat. Assoc.* **1968**, *39*, 1379–1389.
33. Longobardi, A.; Villani, P. Trend Analysis of annual and seasonal rainfall time series in the Mediterranean area. *Int. J. Climatol.* **2010**, *30*, 1538–1546.
34. Chen, D. A monthly circulation climatology for Sweden and its application to a winter temperature case study. *Int. J. Climat.* **2000**, *20*, 1067–1076.
35. Tošić, I.; Putniković, S.; Tošić, M.; Lazić, I. Extreme Temperature Events in Serbia in Relation to Atmospheric Circulation. *Atmosphere* **2021**, *12*, 1584. https://doi.org/10.3390/atmos12121584.
36. Ma, N.; Zhang, Y. Increasing Tibetan Plateau terrestrial evapotranspiration primarily driven by precipitation. *Agr. Forest. Meteorol.* **2022**, *317*, 108887. https://doi.org/10.1016/j.agrformet.2022.108887.
37. Samuels, R.; Hochman, A.; Baharad, A.; Givati, A.; Levi, Y.; Yosef, Y.; Saaroni, H.; Ziv, B.; Harpaz, T.; Alpert, P. Evaluation and projection of extreme precipitation indices in the Eastern Mediterranean based on CMIP5 multi-model ensemble. *Int. J. Climat.* **2018**, *38*, 2280–2297. https://doi.org/10.1002/joc.5334.
38. Qiu, Y.; Feng, J.; Yan, Z.; Wang, J.; Li, Z. High-resolution dynamical downscaling for regional climate projection in Central Asia based on bias-corrected multiple GCMs. *Clim. Dyn.* **2022**, *58*, 777–791. https://doi.org/10.1007/s00382-021-05934-2.
39. Hui, P.; Wei, F.; Xiao, Y.; Yang, J.; Xu, J.; Tang, J. Future projection of extreme precipitation within CORDEX East Asia phase II: Multi-model ensemble. *Theor. Appl. Climatol.* **2022**. https://doi.org/10.1007/s00704-022-04223-0.